

# Axion Like Particle Search at Higgs Factories

Kingman Cheung,<sup>a,b,c</sup> C.J. Ouseph<sup>a,b</sup>

<sup>a</sup> *Department of Physics, National Tsing Hua University, Hsinchu 30013, Taiwan*

<sup>b</sup> *Center for Theory and Computation,*

*National Tsing Hua University, Hsinchu 30013, Taiwan*

<sup>c</sup> *Division of Quantum Phases and Devices, School of Physics,*

*Konkuk University, Seoul 143-701, Republic of Korea*

(Dated: March 30, 2023)

## Abstract

We study the potential of the future Higgs factories, including the ILC, CEPC, and FCC-ee with  $\sqrt{s} = 240\text{-}250$  GeV on discovering axion-like particles (ALPs) through various production channels in the leptonic final states,  $e^+e^- \rightarrow f\bar{f}a$ , where  $f = e, \mu, \nu$ . We show that the  $e^+e^- \rightarrow e^+e^-a$  with  $a \rightarrow \gamma\gamma$  provides the best bounds for the  $g_{a\gamma\gamma}$  and  $g_{aZZ}$  couplings, while  $e^+e^- \rightarrow \nu\bar{\nu}a$ , with  $a \rightarrow \gamma\gamma$  offers the best bounds for the  $g_{aZZ}$  and  $g_{aZ\gamma}$  couplings. The  $e^+e^- \rightarrow \mu^+\mu^-a$  with  $a \rightarrow \gamma\gamma$  provides intermediate sensitivity to the  $g_{aZZ}$  coupling. Our estimates of the bounds for the  $g_{a\gamma\gamma}$ ,  $g_{aZ\gamma}$ , and  $g_{aZZ}$  couplings as a function of ALP mass ( $M_a$ ) ranging from 0.1 GeV to 100 GeV provide valuable insights for future experiments aiming to detect ALPs. We find that  $g_{a\gamma\gamma}$  around  $1.5 \times 10^{-4}$  GeV<sup>-1</sup> for  $M_a = 0.1 - 6$  GeV is currently not ruled out by any other experiments.

## I. INTRODUCTION

The strong CP problem in the standard model (SM) is a long-standing problem [1]. The best solution comes by introducing a global  $U(1)_{PQ}$  symmetry, which was spontaneously broken down by a dynamical axion field. The resulting pseudo-Nambu-Goldstone boson is known as the QCD axion [1–3]. It can also serve as a dark matter candidate [4–6].

Nonobservation of the neutron electric dipole moment demands the breaking scale of the PQ symmetry to be very high with  $f_a > 10^9$  GeV, implying a tiny mass to the axion and very small couplings to the SM particles. If we do not require the pseudo-Nambu-Goldstone boson to be the solution of the strong CP problem, the mass of the axion is not restricted by the breaking scale  $f_a$ . Such a hypothetical particle, coined as axion-like particle (ALP), is also a pseudoscalar boson.

However, the ALP remains one of the possible dark matter candidates. The axion mass and couplings to SM particles can extend over many orders of magnitude, which are only constrained by astrophysical and cosmological observations, as well as collider experiments. In this work, we consider the potential sensitivities on the parameter space of the ALP model by searching for such ALPs in the proposed Higgs factories, including the International Linear Collider (ILC) [7], CEPC [8], and FCC-ee [9] with  $\sqrt{s} = 240 - 250$  GeV. We consider the following leptonic production channels  $e^+e^- \rightarrow f\bar{f}a$  with  $f = e, \mu, \nu$ . Given the center-of-mass energy is only 250 GeV, we consider the ALP mass in the range of 0.1 – 100 GeV. Typical Feynman diagrams for production can be found in Fig. 1.

We focus on the diphoton decay mode of the ALP, which is shown to be dominant. Thus, we have rather clean final states  $f\bar{f}(\gamma\gamma)$  with  $f = e, \mu, \nu$ . The SM background is calculated and found to be small. Finally, we show the sensitive regions of the couplings. The organization of this work is as follows. In the next section, we describe the model and existing constraints. In Sec. III, we show the signal-background analysis. We calculate the sensitivities of the ALP couplings in Sec. IV. We summarize in Sec. V.

## II. THEORETICAL SETUP

### A. Model

The axion, as a pseudo-Goldstone boson, has derivative couplings to fermions, as well as  $CP$ -odd couplings to the gauge field strengths. Before rotating the  $B$  and  $W^i$  fields to the physical  $\gamma$ ,  $Z$ ,  $W^\pm$ , the interactions of the axion are given by [10–12]

$$\mathcal{L} = \mathcal{L}_f + \mathcal{L}_g + \mathcal{L}_{BB} + \mathcal{L}_{WW} \quad (1)$$

where,

$$\begin{aligned} \mathcal{L}_f &= -\frac{ia}{f_a} \sum_f g_{af} m_f^{diag} \bar{f} \gamma_5 f \\ \mathcal{L}_g &= -C_g \frac{a}{f_a} G_{\mu\nu}^A \tilde{G}^{\mu\nu,A} \\ \mathcal{L}_{BB} &= -C_{BB} \frac{a}{f_a} B_{\mu\nu} \tilde{B}^{\mu\nu} \\ \mathcal{L}_{WW} &= -C_{WW} \frac{a}{f_a} W_{\mu\nu}^i \tilde{W}^{\mu\nu,i}. \end{aligned}$$

where  $a$  represents the ALP field,  $f_a$  is the ALP decay constant,  $A = 1, \dots, 8$  is the  $SU(3)$  color index and  $i = 1, 2, 3$  is the  $SU(2)$  index. The  $B, W^3$  fields rotated into  $\gamma, Z$  by

$$\begin{pmatrix} W_\mu^3 \\ B_\mu \end{pmatrix} = \begin{pmatrix} c_w & s_w \\ -s_w & c_w \end{pmatrix} \begin{pmatrix} Z_\mu \\ A_\mu \end{pmatrix}. \quad (2)$$

where  $c_w, s_w$  are cosine and sine of the Weinberg angle. The axion interactions with the fermion and the physical gauge bosons are given by

$$\begin{aligned} \mathcal{L} &= -\frac{ia}{f_a} \sum_f g_{af} m_f^{diag} \bar{f} \gamma_5 f - C_g \frac{a}{f_a} G_{\mu\nu}^A \tilde{G}^{\mu\nu,A} - \frac{a}{f_a} [(C_{BB} c_w^2 + C_{WW} s_w^2) F_{\mu\nu} \tilde{F}^{\mu\nu} + \\ & (C_{BB} s_w^2 + C_{WW} c_w^2) Z_{\mu\nu} \tilde{Z}^{\mu\nu} + 2(C_{WW} - C_{BB}) c_w s_w F_{\mu\nu} \tilde{Z}^{\mu\nu} + C_{WW} W_{\mu\nu}^+ \tilde{W}^{-\mu\nu}] \end{aligned} \quad (3)$$

The dimensionful couplings associated with ALP interactions from 3 is given by;

$$g_{a\gamma\gamma} = \frac{4}{f_a} (C_{BB} c_w^2 + C_{WW} s_w^2), \quad (4)$$

$$g_{aWW} = \frac{4}{f_a} C_{WW}, \quad (5)$$

$$g_{aZZ} = \frac{4}{f_a} (C_{BB} s_w^2 + C_{WW} c_w^2), \quad (6)$$

$$g_{aZ\gamma} = \frac{8}{f_a} s_w c_w (C_{WW} - C_{BB}). \quad (7)$$

## B. Existing Constraints on ALPs

The experimental bounds on the couplings of ALP to gluons, photons, weak gauge bosons, and fermions have been thoroughly investigated in numerous sources [13–21], including their effects at colliders when  $f_a$  is approximately at the TeV scale [19, 22]. Moreover, more recent works had constrained the coupling of ALPs to the  $W^\pm$  gauge boson can be found in Ref. [23, 24].

- The LEP and the current LHC experiments can probe a significant region of parameter space for ALPs with mass  $M_a \geq 5\text{GeV}$ . The LEP utilized the  $e^+e^- \rightarrow \gamma a$ , ( $a \rightarrow \gamma\gamma$ ) and  $Z \rightarrow a\gamma$  processes [22] to search for ALPs, while ATLAS and CMS employed the process  $\gamma\gamma \rightarrow a \rightarrow \gamma\gamma$  in PbPb collisions at the LHC [25]. In addition, the rare decay of the Higgs boson  $h \rightarrow Za$ , ( $a \rightarrow \gamma\gamma$ ) and  $h \rightarrow aa \rightarrow (\gamma\gamma)(\gamma\gamma)$  at the LHC [26] had been utilized to explore the ALP-photon coupling  $g_{a\gamma\gamma}$  in relation to the ALP mass  $M_a$ .
- The ALPs with masses below the MeV scale has been extensively studied in cosmological and astrophysical observations, which have resulted in numerous constraints on ALP couplings, including BBN, CMB, and Supernova 1987A [15, 27]. Furthermore, light ALPs can potentially become the cold dark matter [4–6], which could lead to their detection through various astrophysical and terrestrial anomalies [28], such as the unexpected X-ray emission line at around 3.5 keV [29] and the excess of electronic recoil events in XENON1T [30]. These results demonstrated the importance of further exploration and investigation into the properties and behavior of ALPs.
- In the mass range of MeV to GeV, ALPs can significantly impact low-energy observables in particle physics. Recent studies in the intensity frontier [24, 31–33] have explored numerous potential search avenues. Examples include lepton-flavor-violating decays [34], rare meson decays [24, 31, 35, 36], and ALP production in beam dump experiments [37]. Furthermore, this range of ALPs has been proposed as a possible explanation for the muon anomalous magnetic moment [32, 38] and may also provide a feasible solution to the Koto anomaly [39]. These findings highlight the importance of continued research into ALPs and their potential implications in particle physics.

$e^+e^-$ Collider	$\sqrt{s}$ (GeV)	Integrated Luminosity ( $\text{fb}^{-1}$ )
ILC	250	2000
CEPC	240	5600
FCC-ee	250	5000

TABLE I: A few proposals of  $e^+e^-$  colliders running as a Higgs factory, at which the center-of-mass energy and integrated luminosity are shown.

- The search for the process  $e^+e^- \rightarrow \gamma a$  with  $a \rightarrow \gamma\gamma$  has recently been conducted by Belle II [40] for the ALP mass ranging between 0.1 GeV and 10 GeV. The data utilized in this search corresponded to an integrated luminosity of  $(445 \pm 3) \text{pb}^{-1}$ , and the mass range explored was  $0.2 \text{ GeV} < M_a < 9.7 \text{ GeV}$ .
- The process  $e^+e^- \rightarrow e^+e^-a$  with  $a \rightarrow \gamma\gamma$  at ILC has recently been studied in Ref. [41–43]. Ref. [42] showed that the ILC running at  $\sqrt{s} = 250 \text{ GeV}$  or  $\sqrt{s} = 500 \text{ GeV}$  can discover ALPs in this range of masses with significantly smaller couplings to the SM than previous experiments, down to  $g_{aBB} = 10^{-3} \text{ TeV}^{-1}$ . Ref. [41] showed that with more than  $10^9$   $Z$  bosons produced in the Giga- $Z$  mode of the future ILC experiment equipped with the high granular nature of the detector, one can discover of the ALPs coupled to hypercharge with couplings down to nearly  $10^{-5} \text{ GeV}^{-1}$  over the mass range from 0.4 to 50 GeV.

A few proposals of Higgs factories are put forward, including the ILC [7], CEPC [8], and FCC-ee [9], running at center-of-energies at  $\sqrt{s} = 240 - 250 \text{ GeV}$  with the nominal luminosities shown in Table I. One of the main goals is to carry out the precision study of the Higgs boson couplings. We investigate the potential search for ALPs  $e^+e^-$  collisions at the Higgs factories. Without loss of generality, we choose  $\sqrt{s} = 250 \text{ GeV}$  and a conservative integrated luminosity of  $2 \text{ ab}^{-1}$ .

At the Higgs factories, the leptonic processes that we consider are  $e^+e^- \rightarrow f\bar{f}a$  where  $f = e, \mu, \text{ or } \nu$ , followed by  $a \rightarrow \gamma\gamma$ . This study explores the effects of the coupling  $g_{a\gamma\gamma}, g_{a\gamma Z}, g_{aZZ}, g_{aWW}$  on the production rates of the ALP. Typical contributing Feynman diagrams are shown in Fig. 1. Among the diagrams, there are  $s$ - and  $t$ -channel diagrams with the ALP bremsstrahlung off an internal  $\gamma, Z$ , or  $W$  propagator.

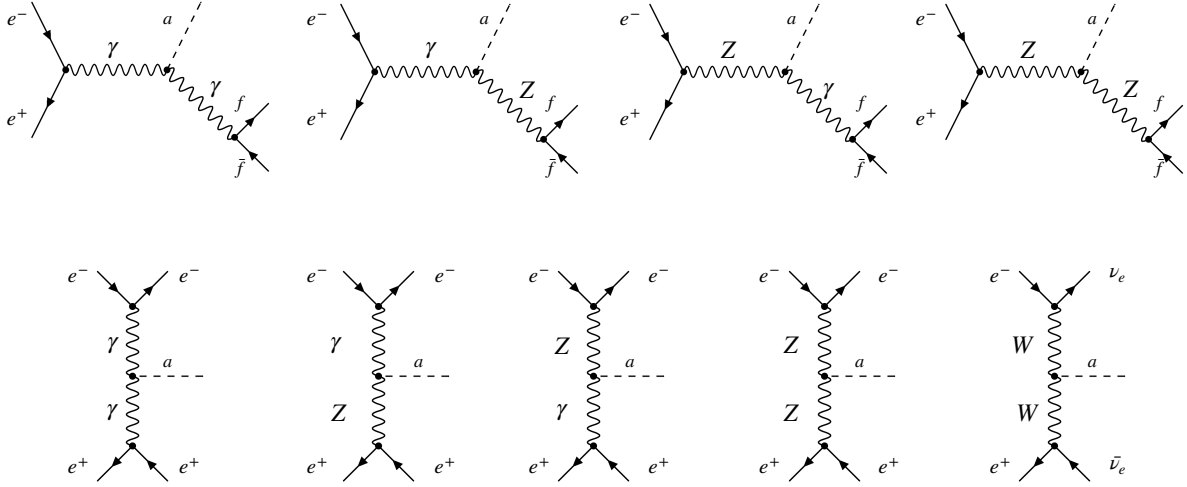


FIG. 1: Typical Feynman diagrams for production of axion-like particles  $a$  via the process

$$e^+e^- \rightarrow f\bar{f}a \text{ at } e^+e^- \text{ collisions, where } f = e, \mu, \nu.$$

### III. SIGNAL VERSUS BACKGROUND

We use MadGraph5aMC@NLO [44, 45] to generate events for the production of ALPs at  $e^+e^-$  collisions. We consider the following channels for detecting the ALP signal:

- $e^+e^- \rightarrow e^+e^-a$  with  $a \rightarrow \gamma\gamma$

To obtain the production cross-sections of the ALP with mass from  $M_a = 0.1$  GeV to 100 GeV, we apply the following initial cuts on the transverse momentum  $p_T^e$  and rapidity  $|\eta^e|$  of the electrons in the final state, as well as the transverse momentum  $p_T^\gamma$  and rapidity  $|\eta^\gamma|$  of the photons in final state.

- $p_{T\min}^e = 10$  GeV
- $|\eta_{\max}^e| = 1.83$  ( $|\cos\theta_e| < 0.95$ )
- $p_{T\min}^\gamma = 10$  GeV
- $|\eta_{\max}^\gamma| = 2.5$

- $e^+e^- \rightarrow \mu^+\mu^-a$  with  $a \rightarrow \gamma\gamma$

The final state consisting of muons ( $\mu^\pm$ ) and a pair of photons from the ALP decay

are selected using the same cuts as the electron case

- $p_{T\min}^\mu = 10 \text{ GeV}$
- $|\eta_{\max}^\mu| = 1.83 \quad (|\cos \theta_\mu| < 0.95)$
- $p_{T\min}^\gamma = 10 \text{ GeV}$
- $|\eta_{\max}^\gamma| = 2.5$

- $e + e^- \rightarrow \nu \bar{\nu} a$  with  $a \rightarrow \gamma\gamma$

Here the ALP is produced along with neutrinos in the final states are selected using the following cuts on the rapidity and transverse momentum of the photon and missing transverse energy of  $E_T$ .

- $/E_T^{\min} = 20 \text{ GeV}$
- $p_{T\min}^\gamma = 10 \text{ GeV}$
- $|\eta_{\max}^\gamma| = 2.5$

The corresponding irreducible background is also subject to the same cuts as discussed above. We use  $C_{WW} = 2$ ,  $C_{BB} = 1$ , and  $f_a = 1 \text{ TeV}$  in calculating the ALP cross sections, so the corresponding coupling strengths  $g_{a\gamma\gamma}$ ,  $g_{aZ\gamma}$ ,  $g_{aZZ}$ , and  $g_{aWW}$  are obtained using Eqs. (4) – (7) and listed in Table II. Note that we have chosen different values for  $C_{WW}$  and  $C_{BB}$ , otherwise  $g_{aZ\gamma}$  would vanish.

TABLE II: The ALP coupling strengths  $g_{a\gamma\gamma}$ ,  $g_{aZ\gamma}$ ,  $g_{aZZ}$ . and  $g_{aWW}$  with  $C_{WW} = 2$ ,  $C_{BB} = 1$ ,  $f_a = 10^3 \text{ GeV}$  using Eqs. (4) – (7).

ALP couplings	Numerical Value ( $\text{GeV}^{-1}$ )
$g_{a\gamma\gamma}$	$4.88 \times 10^{-3}$
$g_{aZ\gamma}$	$1.38 \times 10^{-3}$
$g_{aZZ}$	$7.11 \times 10^{-3}$
$g_{aWW}$	$8 \times 10^{-3}$

We generated  $10^5$  events using MadGraph5aMC@NLO. The scattering cross-section associated with the process  $e^+e^- \rightarrow f\bar{f}a$  is presented in Fig.2, where  $f = e, \mu, \nu$ . We have

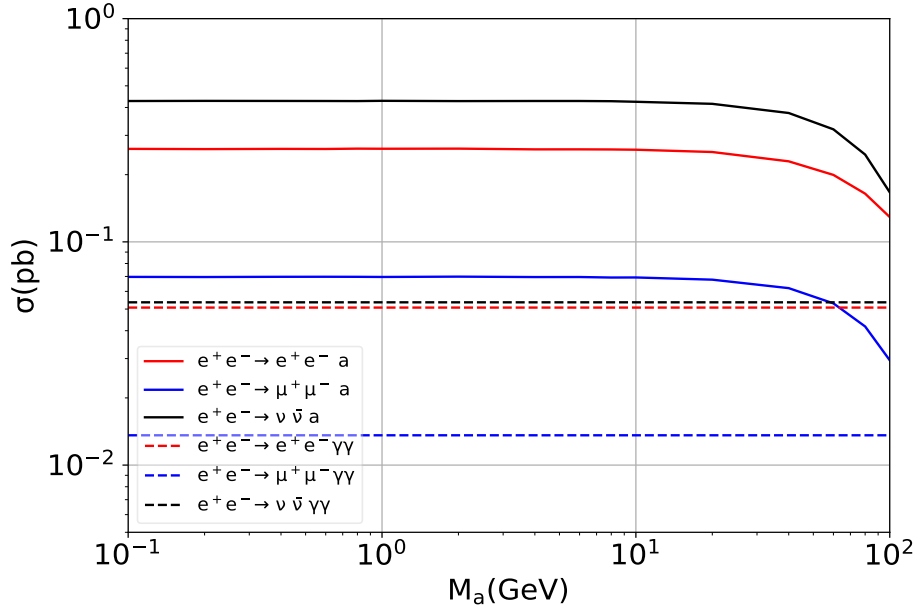


FIG. 2: The ALP signal and SM cross-sections at the Higgs factory with  $\sqrt{s} = 250$  GeV. Signal cross-sections are calculated with the coupling strengths listed in Table. II:

$$g_{a\gamma\gamma} = 4.88 \times 10^{-3} \text{ GeV}^{-1}, g_{aZ\gamma} = 1.38 \times 10^{-3} \text{ GeV}^{-1}, g_{aZZ} = 7.11 \times 10^{-3} \text{ GeV}^{-1}, \text{ and } g_{aWW} = 8 \times 10^{-3} \text{ GeV}^{-1}.$$

computed the cross-sections using the coupling strengths listed in Table II. Among the three signal processes,  $e^+e^- \rightarrow \nu\bar{\nu}a$  has the largest cross-sections, as it consists of three flavors of neutrinos. On the other hand,  $e^+e^- \rightarrow \mu^+\mu^-a$  gives the smallest cross sections. For  $M_a$  ranging from 0.1 GeV to 10 GeV, the cross-section curves remain flat. As  $M_a$  increases from 10 GeV, the cross sections gradually decrease, because the final state phase space becomes limited with increasing ALP mass. This pattern is consistent across all three channels.

To suppress the irreducible background, we apply a cut on the transverse momentum of the photon pair. In Fig. 3, we compare the transverse momentum of the photon pair for  $M_a = 0.1 - 100$  GeV with the corresponding background. A selection cut of  $p_{T,\gamma\gamma} > 50$  GeV can suppress the SM background.

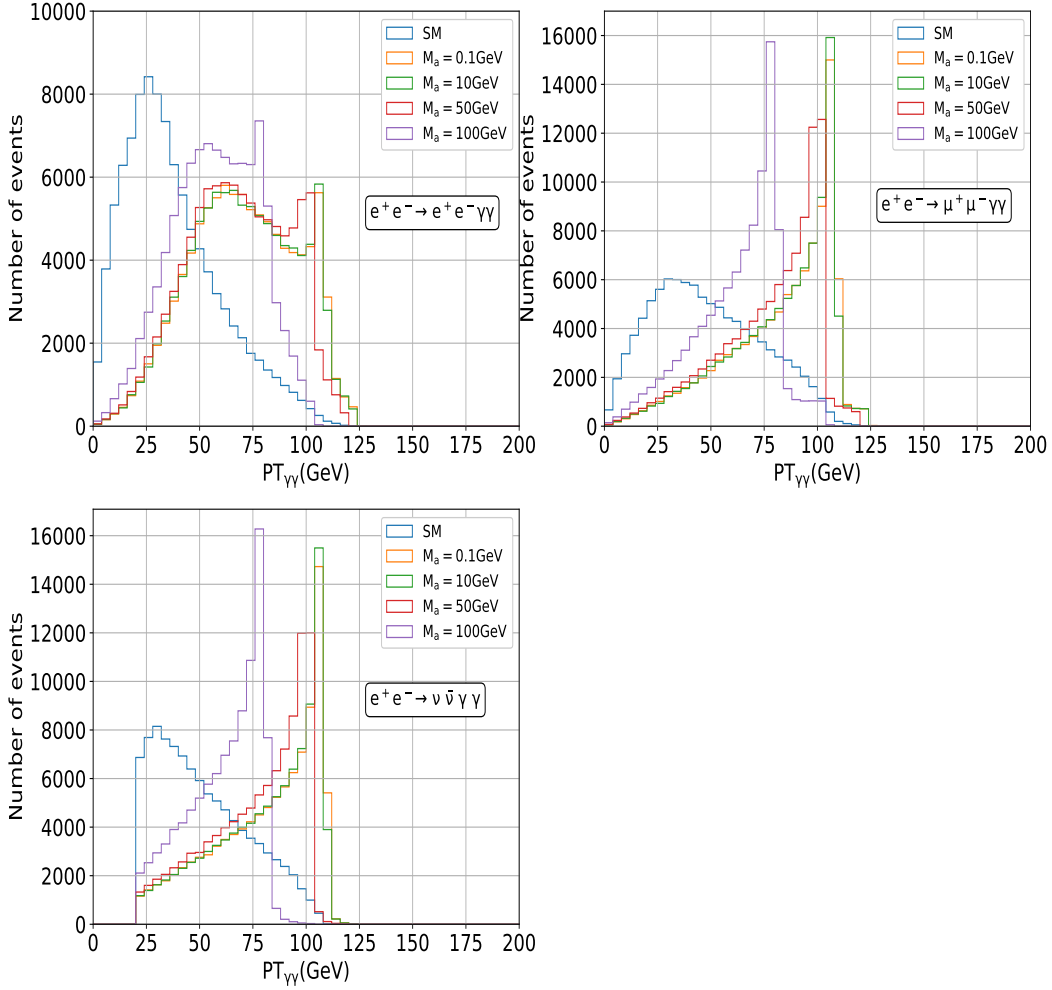


FIG. 3: Transverse momentum  $p_{T,\gamma\gamma}$  distributions of the photon pair for the signal processes with  $M_a = 0.1 - 100$  GeV and the corresponding SM background at  $e^+e^-$  colliders with  $\sqrt{s} = 250$  GeV.

#### IV. SENSITIVITY ON THE ALP MODEL

The number of signal events  $N_T$  at  $e^+e^-$  colliders with  $\sqrt{s} = 250$  GeV is estimated as

$$N_T = \sigma(e^+e^- \rightarrow f\bar{f}a) \times B(a \rightarrow \gamma\gamma) \times \frac{N(p_{T,\gamma\gamma} > 50 \text{ GeV})}{N_{\text{sim}}} \times \mathcal{L}, \quad (8)$$

where  $\sigma(e^+e^- \rightarrow f\bar{f} a)$  is the ALP production cross-section,  $B(a \rightarrow \gamma\gamma)$  is the branching ratio of the ALP to a pair of photons (see Appendix),  $N(p_{T\gamma\gamma} > 50 \text{ GeV})$  is the number of events surviving the  $p_{T\gamma\gamma} > 50 \text{ GeV}$  cut, and  $N_{\text{sim}}$  is the total number of events simulated. In this study, we generated  $N_{\text{sim}} = 10^5$  events using MadGraph5aMC@NLO and  $\mathcal{L}$  is the integrated luminosity, which we conservatively choose  $\mathcal{L} = 2 \text{ ab}^{-1}$ . Similarly, the number of background events  $N_T^{\text{SM}}$  is estimated as

$$N_T^{\text{SM}} = \sigma(e^+e^- \rightarrow f\bar{f} \gamma\gamma) \times \frac{N(p_{T\gamma\gamma} > 50 \text{ GeV})}{N_{\text{sim}}} \times \mathcal{L}. \quad (9)$$

The number of signal events  $N_T$  is proportional to the square of the ALP coupling strength  $g$ . In this study, we consider all possible ALP interactions encoded in Eq. (3), from all possible channels of ALP production listed in Fig. 1. The bound on the ALP coupling as a function of ALP mass can be obtained by requiring the significance  $Z > 2$ . The significance  $Z$  is defined as [46]:

$$Z = \sqrt{2 \cdot \left[ (s+b) \ln \left( \frac{(s+b)(b+\sigma_b^2)}{b^2 + (s+b)\sigma_b^2} \right) - \frac{b^2}{\sigma_b^2} \ln \left( 1 + \frac{\sigma_b^2 s}{b(b+\sigma_b^2)} \right) \right]}, \quad (10)$$

where the numbers of signal and background events are represented by  $s$  and  $b$ , respectively. The systematic uncertainty associated with the SM background  $b$  is denoted by  $\sigma_b$ . A significance value of  $Z = 2$  is considered, which corresponds to 95% confidence level (C.L.). In the following subsections, we discuss the sensitivity of the ALP couplings from ALP production with three different leptonic final states at the Higgs factory.

#### A. $e^+e^- \rightarrow e^+e^- a$ , $a \rightarrow \gamma\gamma$

The process of ALP production, in conjunction with a pair of electrons mediated by  $\gamma$  and  $Z$  bosons, is illustrated in Fig.1. In this process, the effective couplings of the ALP to  $ZZ$ ,  $\gamma\gamma$ , and  $\gamma Z$  are associated with the dimensional couplings  $g_{aZZ}$ ,  $g_{a\gamma\gamma}$ , and  $g_{aZ\gamma}$ , respectively. The numbers of signal and background events are estimated using Eqs. (8) and (9), and are shown in the left panel of Fig. 4.

The combination of production via photon fusion followed by the ALP decay into diphoton yields the highest number of signal events for the specified value of  $g_{a\gamma\gamma}$  coupling listed in Table. II. The number of ALP events from the ALP- $ZZ$  vertex is intermediate, while the ALP- $Z\gamma$  vertex gives the least number of events, even the SM event rate is higher than the

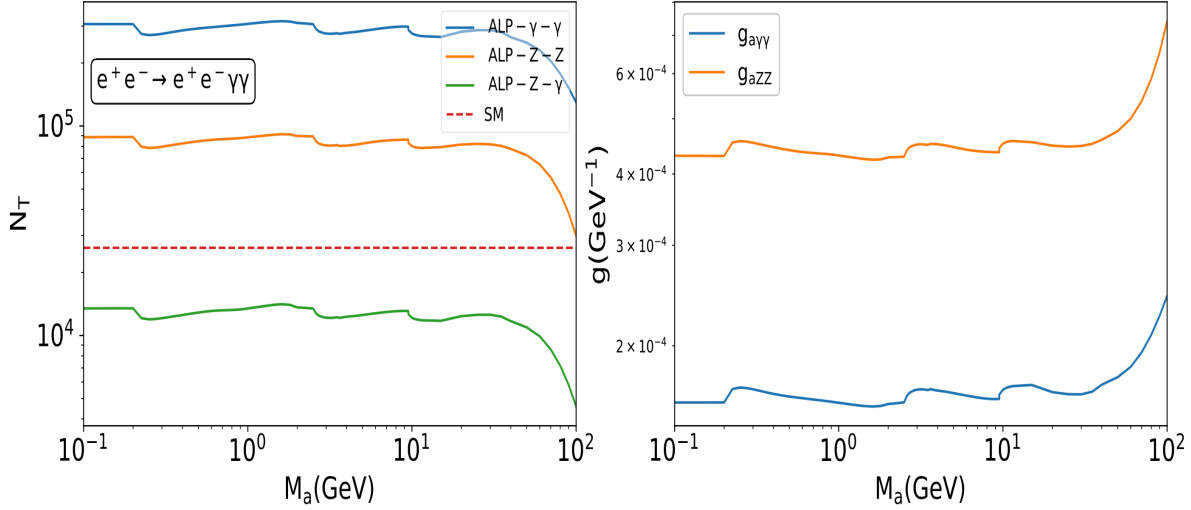


FIG. 4: Left panel: The number of ALP events from the channel  $e^+e^- \rightarrow e^+e^-a$  followed by  $a \rightarrow \gamma\gamma$  (event rates are estimated with the coupling strengths listed in Table. II:  $g_{a\gamma\gamma} = 4.88 \times 10^{-3} \text{ GeV}^{-1}$ ,  $g_{aZ\gamma} = 1.38 \times 10^{-3} \text{ GeV}^{-1}$ , and  $g_{aZZ} = 7.11 \times 10^{-3} \text{ GeV}^{-1}$ ). Right panel: The 95% C.L. sensitivity curves on  $g_{a\gamma\gamma}$  (solid blue) and  $g_{aZZ}$  (solid orange) for  $e^+e^- \rightarrow e^+e^-a$ ,  $a \rightarrow \gamma\gamma$ .

latter one. The kinks in the number of signal event curves arise from the branching ratio of the ALP into diphoton  $a \rightarrow \gamma\gamma$ .

We then estimate the sensitivity in the ALP couplings versus the ALP mass, especially  $g_{a\gamma\gamma}$  and  $g_{aZZ}$  using Eq. (10). We account for the systematic uncertainty associated with the background estimation by including assuming an uncertainty of  $\sigma_b = 10\%$ . The bounds on the ALP couplings  $g_{a\gamma\gamma}$  (blue) and  $g_{aZZ}$  (orange) as a function of the ALP mass  $M_a$  are shown in the right panel of Fig. 4. It is easy to see that the sensitivity of the  $g_{a\gamma\gamma}$  coupling is a few times better than the  $g_{aZZ}$  coupling. At lighter ALP mass of  $M_a = 0.1$  GeV, the sensitivity of  $g_{a\gamma\gamma}$  can reach down to  $\sim 1.5 \times 10^{-4} \text{ GeV}^{-1}$ , while  $g_{aZZ}$  reaches down to  $\sim 4.3 \times 10^{-4} \text{ GeV}^{-1}$ . The sensitivity curves stay more or less flat until  $M_a = 30$  GeV with some irregularities due to the branching ratio into diphoton. As  $M_a$  increases beyond 30 GeV, the sensitivity is largely worsened due to smaller phase space for the production of heavier ALPs. At  $M_a = 100$  GeV, the bounds on  $g_{a\gamma\gamma}$  and  $g_{aZZ}$  are reduced to approximately  $2.5 \times 10^{-4} \text{ GeV}^{-1}$  and  $7.5 \times 10^{-4} \text{ GeV}^{-1}$ , respectively.

**B.**  $e^+e^- \rightarrow \mu^+\mu^-a$ ,  $a \rightarrow \gamma\gamma$

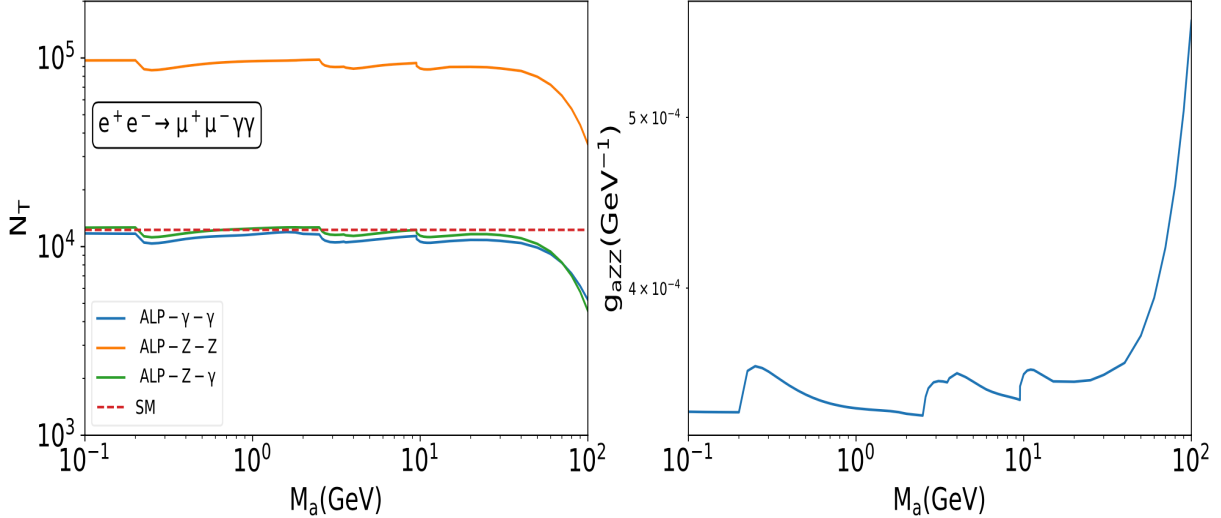


FIG. 5: Left panel: The number of ALP events from the channel  $e^+e^- \rightarrow \mu^+\mu^-a$  followed by  $a \rightarrow \gamma\gamma$  (event rates are estimated with the coupling strengths listed in Table. II:  $g_{a\gamma\gamma} = 4.88 \times 10^{-3} \text{ GeV}^{-1}$ ,  $g_{aZ\gamma} = 1.38 \times 10^{-3} \text{ GeV}^{-1}$ , and  $g_{aZZ} = 7.11 \times 10^{-3} \text{ GeV}^{-1}$ ). Right panel: The 95% C.L. sensitivity curve of  $g_{aZZ}$  (solid blue) for  $e^+e^- \rightarrow \mu^+\mu^-a$ ,  $a \rightarrow \gamma\gamma$ .

Here we consider the associated production of the ALP with a  $\mu^+\mu^-$  pair. This process only arises from  $s$ -channel diagrams listed in Fig. 1. The left panel of Fig. 5 shows the number of ALP events arising from various ALP vertices. The highest number of ALP events comes from ALP production associated with the ALP-ZZ vertex. The numbers of ALP events produced via the ALP-Z $\gamma$  and ALP- $\gamma\gamma$  vertices are lower than that of the SM. The right panel of Fig.5 shows the sensitivity reach of the  $g_{aZZ}$  coupling as a function of ALP mass  $M_a$ . The effect of the diphoton branching ratio also reflects in the sensitivity curves. At  $M_a = 0.1 \text{ GeV}$ ,  $g_{aZZ}$  can be probed down to  $\sim 3.4 \times 10^{-4} \text{ GeV}^{-1}$ . The sensitivity of  $g_{aZZ}$  weakens with the increment of the ALP mass, especially for  $M_a$  above 30 GeV.

Comparing the bounds of  $g_{aZZ}$  obtained in the channels  $e^+e^- \rightarrow \mu^+\mu^-a$  (Fig. 5) and  $e^+e^- \rightarrow e^+e^-a$  (Fig. 4), we can see that  $g_{aZZ}$  from the muon channel performs better than the electron channel over the entire ALP mass range. This is simply because the background in the muon channel is only a fraction of the electron channel.

C.  $e^+e^- \rightarrow \nu\bar{\nu}a$ ,  $a \rightarrow \gamma\gamma$

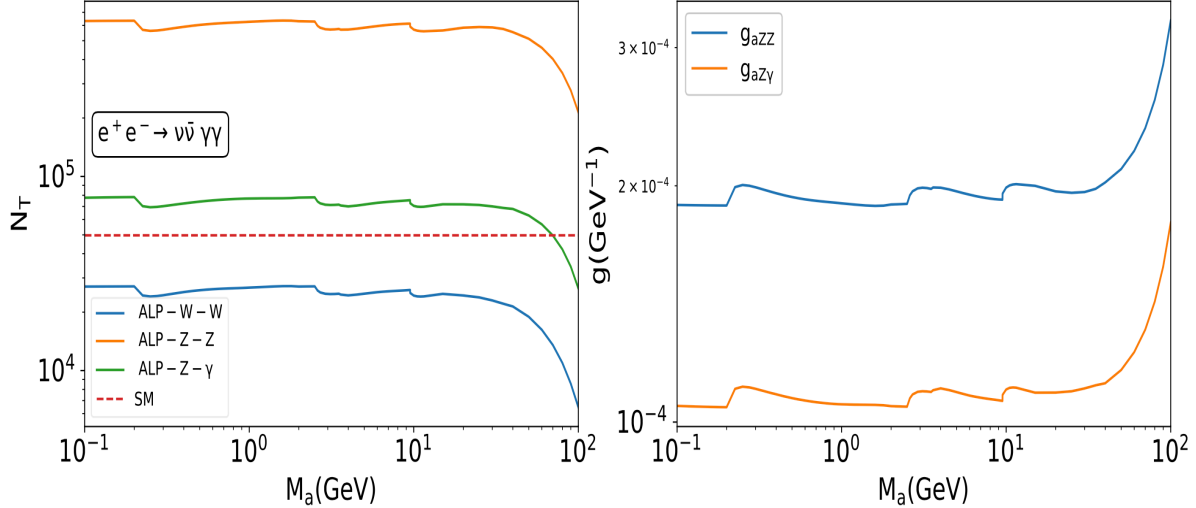


FIG. 6: Left panel: The number of ALP events from  $e^+e^- \rightarrow \nu\bar{\nu}a$ , followed by  $a \rightarrow \gamma\gamma$  (event rates are estimated with the coupling strengths listed in Table. II:  $g_{aZ\gamma} = 1.38 \times 10^{-3}$  GeV $^{-1}$ ,  $g_{aZZ} = 7.11 \times 10^{-3}$  GeV $^{-1}$ , and  $g_{aWW} = 8 \times 10^{-3}$  GeV $^{-1}$ ). Right panel: The 95% C.L. sensitivity curves on  $g_{aZZ}$  (solid blue) and  $g_{aZ\gamma}$  (solid orange) for  $e^+e^- \rightarrow \nu\bar{\nu}a$ ,  $a \rightarrow \gamma\gamma$ .

As already shown in Fig. 2, the channel  $e^+e^- \rightarrow \nu\bar{\nu}a$  with  $a \rightarrow \gamma\gamma$  has the largest cross-sections compared to the other two processes. This process also presents an opportunity to investigate the ALP- $WW$  vertex. In addition to the ALP- $WW$  vertex, the ALP- $ZZ$  and ALP- $Z\gamma$  vertices also make contributions, which are depicted in Fig. 1.

The number of ALP events from the ALP- $ZZ$  vertex is higher than that from the other two vertices. The ALP production rate from the ALP- $WW$  vertex is the lowest and is even lower than that of the SM.

The bounds on  $g_{aZZ}$  and  $g_{aZ\gamma}$  couplings are shown in the right panel of Fig.6. In this case, the  $g_{aZ\gamma}$  coupling has a better bound compared to the  $g_{aZZ}$  coupling. At  $M_a=0.1$  GeV, the  $g_{aZ\gamma}$  coupling can reach down to  $\sim 10^{-4}$  GeV $^{-1}$ , while the  $g_{aZZ}$  coupling reaches down to  $1.8 \times 10^{-4}$  GeV $^{-1}$ . Similar to previous cases, the sensitivity of the couplings weakens as the ALP mass  $M_a$  increases.

When comparing the bounds of  $g_{aZZ}$  coupling obtained from all different channels the best sensitivity comes from  $e^+e^- \rightarrow \nu\bar{\nu}a$ ,  $a \rightarrow \gamma\gamma$ . At  $M_a=0.1$  GeV, the  $g_{aZZ}$  coupling

reaches down to  $1.8 \times 10^{-4} \text{GeV}^{-1}$ . The  $e^+e^- \rightarrow e^+e^-a$ ,  $a \rightarrow \gamma\gamma$  channel offers the least sensitivity (for  $M_a=0.1 \text{ GeV}$   $g_{aZZ}$  coupling only reaches down to  $4.3 \times 10^{-4} \text{GeV}^{-1}$ ). The limit from the  $e^+e^- \rightarrow \mu^+\mu^-a$ ,  $a \rightarrow \gamma\gamma$  channel is intermediate (for  $M_a=0.1 \text{ GeV}$  the  $g_{aZZ}$  coupling reaches down to  $3.4 \times 10^{-4} \text{GeV}^{-1}$ ). This trend is visible across the entire ALP mass range from  $M_a = 0.1 \text{ GeV}$  to  $100 \text{ GeV}$ .

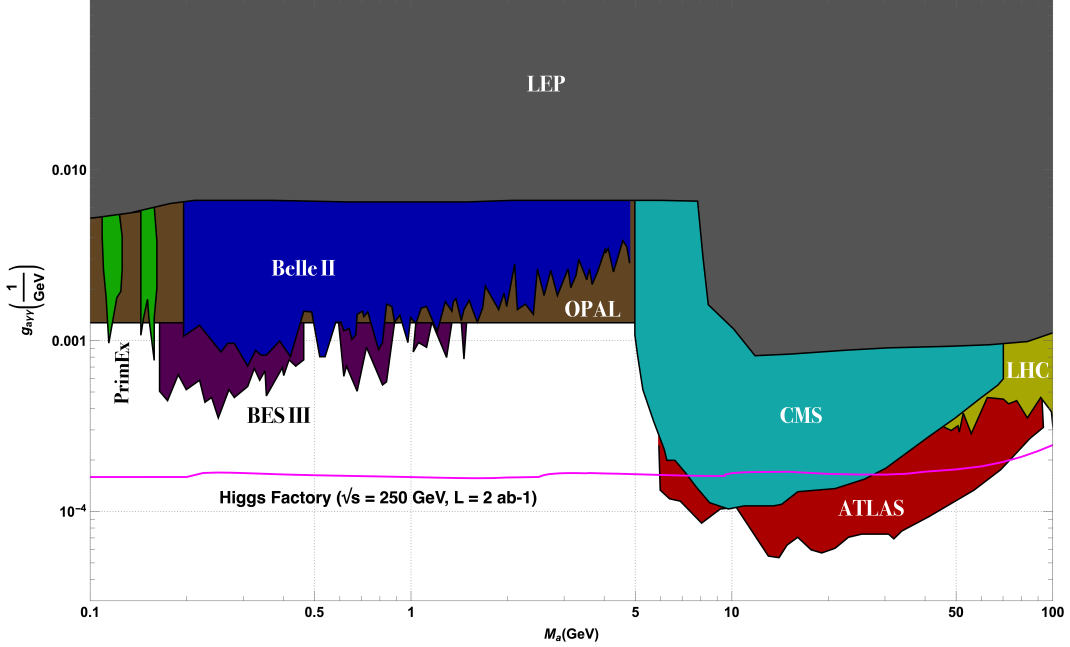


FIG. 7: Summary plot of the sensitivity of  $g_{a\gamma\gamma}$  that we can achieve at the Higgs factory  $\sqrt{s} = 250 \text{ GeV}$  with an integrated luminosity  $2 \text{ ab}^{-1}$ , and compared with other existing constraints. Existing constraints in the figure include PrimEx [47], BES III [48], Belle II[40], LEP [22], OPAL [49], CMS [50], ATLAS [51] and LHC [49] (extracted from the GitHub page [52]).

## V. CONCLUSIONS

In this study, we have explored the sensitivity potential of the future Higgs factories, including ILC, CEPC, and FCC-ee, on probing dimensionful coupling constants  $g_{a\gamma\gamma}$ ,  $g_{aZ\gamma}$ ,  $g_{aWW}$ , and  $g_{aZZ}$  of the axion-like particle, via the processes  $e^+e^- \rightarrow f\bar{f}a$  ( $f = e, \mu, \nu$ ) followed by  $a \rightarrow \gamma\gamma$ . We used a center-of-mass energy  $\sqrt{s} = 250 \text{ GeV}$  with an integrated

luminosity  $2 \text{ ab}^{-1}$ .

Our results have shown that the channel  $e^+e^- \rightarrow e^+e^-a$ ,  $a \rightarrow \gamma\gamma$  provides the best bound for the  $g_{a\gamma\gamma}$  coupling, while the process  $e^+e^- \rightarrow \nu\bar{\nu}a$ ,  $a \rightarrow \gamma\gamma$  offers the best bound for the  $g_{aZZ}$  and  $g_{aZ\gamma}$  couplings.

Without loss of generality, we have used  $C_{WW} = 2$  and  $C_{BB} = 1$  such that  $g_{a\gamma\gamma}$ ,  $g_{aZ\gamma}$ ,  $g_{aWW}$ , and  $g_{aZZ}$  are related to one another shown in Eqs. (4) – (7), and they are all nonzero. We can easily extend the analysis to independent coupling strengths.

Finally, we show in Fig. 7 the summary plot of the sensitivity of  $g_{a\gamma\gamma}$  that we can achieve at the Higgs factories, and compared with other existing constraints. The sensitivity can improve down to about  $1.5 \times 10^{-4} \text{ GeV}^{-1}$  over the mass range of  $M_a = 0.1 - 6 \text{ GeV}$ , as well as a small corner at  $M_a \simeq 70 - 100 \text{ GeV}$ .

Our estimates of the bounds for the  $g_{a\gamma\gamma}$ ,  $g_{aZ\gamma}$ , and  $g_{aZZ}$  couplings as a function of ALP mass ( $M_a$ ) ranging from 0.1 GeV to 100 GeV provide valuable insights for future experiments aiming to detect ALPs.

## Appendix A: Partial Decay Widths and Branching Ratios of the ALP

The two-body partial decay widths of the ALP to photons and fermions are given below. The branching ratios are evaluated with  $C_{BB} = 1$ ,  $C_{WW} = 2$ ,  $c_{a\phi} = 1$  and  $f_a = 1000 \text{ GeV}$ . Here  $M_l$  and  $M_q$  are the masses of charged leptons and quarks.

$$\Gamma(a \rightarrow \gamma\gamma) = \frac{M_a^6 (C_{BB}c_w^2 + C_{WW}s_w^2)^2}{4f_a^2\pi|M_a^3|}, \quad (\text{A1})$$

$$\Gamma(a \rightarrow l\bar{l}) = \frac{c_{a\phi}^2 M_a^2 \sqrt{M_a^2 - 4M_a^2 M_l^2} vev^2 y_l^2}{16\pi f_a^2 |M_a^3|} \quad (\text{A2})$$

$$\Gamma(a \rightarrow q\bar{q}) = \frac{3 c_{a\phi}^2 M_a^2 \sqrt{M_a^2 - 4M_a^2 M_q^2} vev^2 y_q^2}{16\pi f_a^2 |M_a^3|} \quad (\text{A3})$$

## ACKNOWLEDGEMENT

Special thanks to Zeren Simon Wang and Nguyen Tran Quang Thong for an enlightening discussion. The work was supported in part by NSTC under the grant number MOST-110-

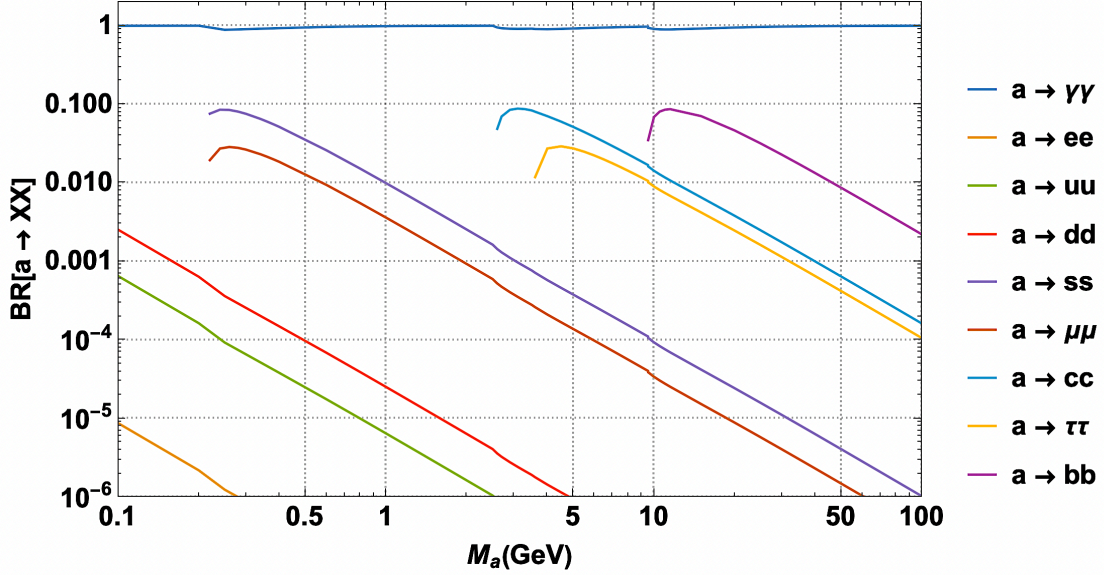


FIG. 8: Branching ratios of the ALP with  $C_{WW} = 2$ ,  $C_{BB} = 1$ , and  $f_a = 1$  TeV.

2112-M-007-017-MY3.

- 
- [1] R. D. Peccei and H. R. Quinn, *CP Conservation in the Presence of Instantons*, *Phys. Rev. Lett.* **38** (1977) 1440–1443.
- [2] S. Weinberg, *A New Light Boson?*, *Phys. Rev. Lett.* **40** (1978) 223–226.
- [3] F. Wilczek, *Problem of Strong P and T Invariance in the Presence of Instantons*, *Phys. Rev. Lett.* **40** (1978) 279–282.
- [4] J. Preskill, M. B. Wise, and F. Wilczek, *Cosmology of the Invisible Axion*, *Phys. Lett. B* **120** (1983) 127–132.
- [5] L. F. Abbott and P. Sikivie, *A Cosmological Bound on the Invisible Axion*, *Phys. Lett. B* **120** (1983) 133–136.
- [6] M. Dine and W. Fischler, *The Not So Harmless Axion*, *Phys. Lett. B* **120** (1983) 137–141.
- [7] ILC Collaboration, G. Aarons et al., *International Linear Collider Reference Design Report Volume 2: Physics at the ILC*, arXiv:0709.1893.
- [8] M. Ahmad et al., *CEPC-SPPC Preliminary Conceptual Design Report. 1. Physics and Detector*, .

- [9] **FCC** Collaboration, A. Abada et al., *FCC-ee: The Lepton Collider: Future Circular Collider Conceptual Design Report Volume 2*, *Eur. Phys. J. ST* **228** (2019), no. 2 261–623.
- [10] I. Brivio, M. B. Gavela, L. Merlo, K. Mimasu, J. M. No, R. del Rey, and V. Sanz, *ALPs Effective Field Theory and Collider Signatures*, *Eur. Phys. J. C* **77** (2017), no. 8 572, [arXiv:1701.05379].
- [11] H. Georgi, D. B. Kaplan, and L. Randall, *Manifesting the Invisible Axion at Low-energies*, *Phys. Lett. B* **169** (1986) 73–78.
- [12] J. Ren, D. Wang, L. Wu, J. M. Yang, and M. Zhang, *Detecting an axion-like particle with machine learning at the LHC*, *JHEP* **11** (2021) 138, [arXiv:2106.07018].
- [13] **Particle Data Group** Collaboration, K. A. Olive et al., *Review of Particle Physics*, *Chin. Phys. C* **38** (2014) 090001.
- [14] N. Vinyoles, A. Serenelli, F. L. Villante, S. Basu, J. Redondo, and J. Isern, *New axion and hidden photon constraints from a solar data global fit*, *JCAP* **10** (2015) 015, [arXiv:1501.01639].
- [15] G. G. Raffelt, *Astrophysical axion bounds*, *Lect. Notes Phys.* **741** (2008) 51–71, [hep-ph/0611350].
- [16] A. Friedland, M. Giannotti, and M. Wise, *Constraining the Axion-Photon Coupling with Massive Stars*, *Phys. Rev. Lett.* **110** (2013), no. 6 061101, [arXiv:1210.1271].
- [17] A. Ayala, I. Domínguez, M. Giannotti, A. Mirizzi, and O. Straniero, *Revisiting the bound on axion-photon coupling from Globular Clusters*, *Phys. Rev. Lett.* **113** (2014), no. 19 191302, [arXiv:1406.6053].
- [18] **CMS** Collaboration, V. Khachatryan et al., *Search for dark matter, extra dimensions, and unparticles in monojet events in proton–proton collisions at  $\sqrt{s} = 8$  TeV*, *Eur. Phys. J. C* **75** (2015), no. 5 235, [arXiv:1408.3583].
- [19] **ATLAS** Collaboration, G. Aad et al., *Search for new phenomena in final states with an energetic jet and large missing transverse momentum in pp collisions at  $\sqrt{s} = 8$  TeV with the ATLAS detector*, *Eur. Phys. J. C* **75** (2015), no. 7 299, [arXiv:1502.01518]. [Erratum: *Eur.Phys.J.C* 75, 408 (2015)].
- [20] **XENON100** Collaboration, E. Aprile et al., *First Axion Results from the XENON100 Experiment*, *Phys. Rev. D* **90** (2014), no. 6 062009, [arXiv:1404.1455]. [Erratum: *Phys.Rev.D* 95, 029904 (2017)].

- [21] N. Viaux, M. Catelan, P. B. Stetson, G. Raffelt, J. Redondo, A. A. R. Valcarce, and A. Weiss, *Neutrino and axion bounds from the globular cluster M5 (NGC 5904)*, *Phys. Rev. Lett.* **111** (2013) 231301, [[arXiv:1311.1669](#)].
- [22] J. Jaeckel and M. Spannowsky, *Probing MeV to 90 GeV axion-like particles with LEP and LHC*, *Phys. Lett. B* **753** (2016) 482–487, [[arXiv:1509.00476](#)].
- [23] M. J. Dolan, F. Kahlhoefer, C. McCabe, and K. Schmidt-Hoberg, *A taste of dark matter: Flavour constraints on pseudoscalar mediators*, *JHEP* **03** (2015) 171, [[arXiv:1412.5174](#)]. [Erratum: *JHEP* 07, 103 (2015)].
- [24] E. Izaguirre, T. Lin, and B. Shuve, *Searching for Axionlike Particles in Flavor-Changing Neutral Current Processes*, *Phys. Rev. Lett.* **118** (2017), no. 11 111802, [[arXiv:1611.09355](#)].
- [25] D. d’Enterria, *Collider constraints on axion-like particles*, in *Workshop on Feebly Interacting Particles*, 2, 2021. [arXiv:2102.08971](#).
- [26] M. Bauer, M. Neubert, and A. Thamm, *LHC as an Axion Factory: Probing an Axion Explanation for  $(g - 2)_\mu$  with Exotic Higgs Decays*, *Phys. Rev. Lett.* **119** (2017), no. 3 031802, [[arXiv:1704.08207](#)].
- [27] D. J. E. Marsh, *Axion Cosmology*, *Phys. Rept.* **643** (2016) 1–79, [[arXiv:1510.07633](#)].
- [28] P. Arias, D. Cadamuro, M. Goodsell, J. Jaeckel, J. Redondo, and A. Ringwald, *WISPy Cold Dark Matter*, *JCAP* **06** (2012) 013, [[arXiv:1201.5902](#)].
- [29] J. Jaeckel, J. Redondo, and A. Ringwald, *3.55 keV hint for decaying axionlike particle dark matter*, *Phys. Rev. D* **89** (2014) 103511, [[arXiv:1402.7335](#)].
- [30] C. Gao, J. Liu, L.-T. Wang, X.-P. Wang, W. Xue, and Y.-M. Zhong, *Reexamining the Solar Axion Explanation for the XENON1T Excess*, *Phys. Rev. Lett.* **125** (2020), no. 13 131806, [[arXiv:2006.14598](#)].
- [31] M. J. Dolan, T. Ferber, C. Hearty, F. Kahlhoefer, and K. Schmidt-Hoberg, *Revised constraints and Belle II sensitivity for visible and invisible axion-like particles*, *JHEP* **12** (2017) 094, [[arXiv:1709.00009](#)]. [Erratum: *JHEP* 03, 190 (2021)].
- [32] M. Bauer, M. Neubert, S. Renner, M. Schnubel, and A. Thamm, *Axionlike Particles, Lepton-Flavor Violation, and a New Explanation of  $a_\mu$  and  $a_e$* , *Phys. Rev. Lett.* **124** (2020), no. 21 211803, [[arXiv:1908.00008](#)].
- [33] **NA64** Collaboration, D. Banerjee et al., *Search for Axionlike and Scalar Particles with the NA64 Experiment*, *Phys. Rev. Lett.* **125** (2020), no. 8 081801, [[arXiv:2005.02710](#)].

- [34] L. Calibbi, D. Redigolo, R. Ziegler, and J. Zupan, *Looking forward to lepton-flavor-violating ALPs*, *JHEP* **09** (2021) 173, [[arXiv:2006.04795](#)].
- [35] F. Björkeröth, E. J. Chun, and S. F. King, *Flavourful Axion Phenomenology*, *JHEP* **08** (2018) 117, [[arXiv:1806.00660](#)].
- [36] S. Chakraborty, M. Kraus, V. Loladze, T. Okui, and K. Tobioka, *Heavy QCD axion in  $b \rightarrow s$  transition: Enhanced limits and projections*, *Phys. Rev. D* **104** (2021), no. 5 055036, [[arXiv:2102.04474](#)].
- [37] B. Döbrich, J. Jaeckel, F. Kahlhoefer, A. Ringwald, and K. Schmidt-Hoberg, *ALPtraum: ALP production in proton beam dump experiments*, *JHEP* **02** (2016) 018, [[arXiv:1512.03069](#)].
- [38] W. J. Marciano, A. Masiero, P. Paradisi, and M. Passera, *Contributions of axionlike particles to lepton dipole moments*, *Phys. Rev. D* **94** (2016), no. 11 115033, [[arXiv:1607.01022](#)].
- [39] S. Gori, G. Perez, and K. Tobioka, *KOTO vs. NA62 Dark Scalar Searches*, *JHEP* **08** (2020) 110, [[arXiv:2005.05170](#)].
- [40] **Belle-II** Collaboration, F. Abudinén et al., *Search for Axion-Like Particles produced in  $e^+e^-$  collisions at Belle II*, *Phys. Rev. Lett.* **125** (2020), no. 16 161806, [[arXiv:2007.13071](#)].
- [41] N. Steinberg and J. D. Wells, *Axion-Like Particles at the ILC Giga-Z*, *JHEP* **08** (2021) 120, [[arXiv:2101.00520](#)].
- [42] N. Steinberg, *Discovering Axion-Like Particles with Photon Fusion at the ILC*, [[arXiv:2108.11927](#)].
- [43] C.-X. Yue, H.-Y. Zhang, and H. Wang, *Production of axion-like particles via vector boson fusion at future electron-positron colliders*, *Eur. Phys. J. C* **82** (2022), no. 1 88, [[arXiv:2112.11604](#)].
- [44] J. Alwall, M. Herquet, F. Maltoni, O. Mattelaer, and T. Stelzer, *MadGraph 5 : Going Beyond*, *JHEP* **06** (2011) 128, [[arXiv:1106.0522](#)].
- [45] J. Alwall, R. Frederix, S. Frixione, V. Hirschi, F. Maltoni, O. Mattelaer, H. S. Shao, T. Stelzer, P. Torrielli, and M. Zaro, *The automated computation of tree-level and next-to-leading order differential cross sections, and their matching to parton shower simulations*, *JHEP* **07** (2014) 079, [[arXiv:1405.0301](#)].
- [46] A. Arhrib, K. Cheung, and C.-T. Lu, *Same-sign charged Higgs boson pair production in bosonic decay channels at the HL-LHC and HE-LHC*, *Phys. Rev. D* **102** (2020), no. 9

- 095026, [arXiv:1910.02571].
- [47] D. Aloni, C. Fanelli, Y. Soreq, and M. Williams, *Photoproduction of Axionlike Particles*, *Phys. Rev. Lett.* **123** (2019), no. 7 071801, [arXiv:1903.03586].
- [48] **BESIII** Collaboration, M. Ablikim et al., *Search for an axion-like particle in radiative  $J/\psi$  decays*, *Phys. Lett. B* **838** (2023) 137698, [arXiv:2211.12699].
- [49] S. Knapen, T. Lin, H. K. Lou, and T. Melia, *Searching for Axionlike Particles with Ultrapерipheral Heavy-Ion Collisions*, *Phys. Rev. Lett.* **118** (2017), no. 17 171801, [arXiv:1607.06083].
- [50] **CMS** Collaboration, A. M. Sirunyan et al., *Evidence for light-by-light scattering and searches for axion-like particles in ultraperipheral PbPb collisions at  $\sqrt{s_{NN}} = 5.02$  TeV*, *Phys. Lett. B* **797** (2019) 134826, [arXiv:1810.04602].
- [51] **ATLAS** Collaboration, G. Aad et al., *Measurement of light-by-light scattering and search for axion-like particles with  $2.2 \text{ nb}^{-1}$  of Pb+Pb data with the ATLAS detector*, *JHEP* **03** (2021) 243, [arXiv:2008.05355]. [Erratum: *JHEP* 11, 050 (2021)].
- [52] C. O’Hare, “cajohare/axionlimits: Axionlimits.”  
<https://cajohare.github.io/AxionLimits/>, July, 2020.